Applied Physics Letters

The effect on the optical modes of quaternary chalcogenides upon metal and chalcogen substitution

Cite as: Appl. Phys. Lett. **116**, 082103 (2020); https://doi.org/10.1063/1.5143248
Submitted: 20 December 2019 . Accepted: 13 February 2020 . Published Online: 26 February 2020

Amanda J. Souna, Kaya Wei, and George S. Nolas

Applied Physics Letters ARTICLE scitation.org/journal/apl

The effect on the optical modes of quaternary chalcogenides upon metal and chalcogen substitution

Cite as: Appl. Phys. Lett. **116**, 082103 (2020); doi: 10.1063/1.5143248
Submitted: 20 December 2019 · Accepted: 13 February 2020 ·
Published Online: 26 February 2020

Amanda J. Souna,[1] Kaya Wei,[2] and George S. Nolas[2,a)]

AFFILIATIONS

[1]Department of Chemistry and Biochemistry, University of Maryland, College Park, Maryland 20742, USA
[2]Department of Physics, University of South Florida, Tampa, Florida 33620, USA

[a)]Author to whom correspondence should be addressed: gnolas@usf.edu

ABSTRACT

Raman-scattering spectra of polycrystalline $Cu_2ZnSnSe_4$, $Ag_2ZnSnSe_4$, and $Cu_2CdSnTe_4$ were investigated in order to investigate the vibrational modes upon substitution on the metal and chalcogen sites. The non-symmetric modes shift dramatically with metal substitution in the kesterite materials, with $Ag_2ZnSnSe_4$ modes shifting by 50 cm^{-1} in comparison with that of $Cu_2ZnSnSe_4$. Tellurium substitution results in a lower frequency of the symmetric modes. Structural data are employed to elucidate our results. These results are intended to provide further insight into these materials as they continue to be of interest for potential thermoelectric and photovoltaic applications.

The search for different materials for clean, renewable energy production is directly related to the discovery of materials with certain properties and suitable structural and transport characteristics.[1] To this end, quaternary chalcogenides encompass one class of materials that continues to be of interest. A large class of materials are understood as quaternary chalcogenides; specifically, compositions known as $I_2-II-IV-VI_4$ (I = Cu or Ag, II = Zn or Cd, IV = Si, Ge, or Sn, and VI = S, Se, or Te) have been investigated for over three decades and can be derived from zinc-blende or wurtzite structured binaries by cation sublattice substitution.[2,3] The compositions with the stannite and kesterite crystal structures are of specific interest as potential thermoelectric, photocatalytic, and photovoltaic materials.[4–9]

There have been substantial property enhancements in these materials for energy-related applications. For example, specific light conversion efficiency and thermoelectric property enhancements have been reported.[8–11] The low thermal conductivity in these materials makes them of interest for thermoelectric applications.[10–14] The particular crystal structure and bonding result in unique properties that can be tuned with specific dopants as well as compositional changes. In addition, seemingly small variations in stoichiometry can lead to great differences in the transport properties within similar structure types.[15,16] As property enhancements continue to be realized and reported for these $I_2-II-IV-VI_4$ semiconductors, interest in developing a fundamental understanding of the effects of structural and chemical variations and bonding in these materials also persists,[15,17] which is the focus of this study.

Herein, we present a spectroscopic analysis of the Raman-active vibrational modes in polycrystalline $Cu_2ZnSnSe_4$, $Ag_2ZnSnSe_4$, and $Cu_2CdSnTe_4$. The Raman spectrum of $Cu_2ZnSnSe_4$, a composition whose Raman-active modes have been reported,[18–21] is used as the "reference" in comparing and identifying variations in the vibrational modes of $Ag_2ZnSnSe_4$ and $Cu_2CdSnTe_4$. $Ag_2ZnSnSe_4$ and $Cu_2CdSnTe_4$ are two compositions whose Raman spectra have not been previously reported. We compare the frequencies of the Raman active modes for all three compositions and employ polarized Raman measurements to assign the symmetries of the observed modes in $Cu_2CdSnTe_4$. Together with the structural properties of these materials, we investigated the change in vibrational frequency with metal and chalcogen substitution in these quaternary chalcogenides.

We prepared phase-pure microcrystalline powders of $Cu_2ZnSnSe_4$ and $Ag_2ZnSnSe_4$ by a solution-phase method,[16] whereby $Cu(OOCCH_3)\cdot H_2O$, $C_2H_3AgO_2$, $Zn(CH_3COO)_2\cdot 2H_2O$, $SnCl_2\cdot 2H_2O$, and Se powder, at a 2:1:1:4 ratio, together with oleylamine were loaded into a three-neck flask on a Schlenk line. They were then mixed at room temperature under a N_2 flow for 10 min followed by degassing under vacuum for 100 min before heating to a reaction temperature of 280 °C for 30 min under N_2 flow for the growth of small crystallites. The flask was then rapidly cooled to room temperature in an ice water

bath. Oleylamine is significant in the synthesis of these quaternary chalcogenides as it acts as a surfactant, solvent, and reducing agent.[16,22,23] $Cu_2CdSnTe_4$ was synthesized by direct reaction of the stoichiometric elements[24] inside a sealed, silica ampoule containing a high-purity nitrogen atmosphere at 0.1 Pa and reacted at 973 K for four days before cooling to room temperature. The reaction product was subsequently ground into fine powder, cold pressed into a pellet, and annealed at 573 K for one week. Phase-pure dense (>96% of theoretical density) polycrystalline specimens were realized by spark plasma sintering ($Cu_2ZnSnSe_4$ and $Ag_2ZnSnSe_4$) at 60 MPa and 310 °C for 10 min with a current pulse ratio of 40:5 ms and hot pressing ($Cu_2CdSnTe_4$) at 150 MPa and 300 °C for 3 h under N_2 flow. The selenium-based compositions had relatively small grain sizes of less than 100 nm, while large grain sizes (several micrometers on average) in the tellurium-based composition allowed for polarized Raman spectroscopic investigations, as will be described below. X-ray diffraction (XRD) analyses were employed to identify the phase purity and composition, using energy dispersive spectroscopy corroborating the XRD results. We note that for the selenium-based kesterite ($I\bar{4}$ symmetry) $I_2-II-IV-VI_4$ materials, only a few meV differentiate the kesterite crystal structure from that of stannite ($I\bar{4}2m$), as has been previously reported.[25] We therefore assigned the structure type based on previously published theoretical analyses[15] that corroborate these results. The case for $Cu_2CdSnTe_4$ is more direct, and the stannite crystal structure can be clearly assigned from both experimental and theoretical analyses.[24] Figure 1 illustrates the kesterite and stannite crystal structures.

Raman spectra were collected using a 532-nm laser with a power of 0.75 mW at the sample and focused with a 0.75 NA objective. The scattered signal was collected through the same objective using a spectrometer, with either a 1200 or 2400 lines/mm grating and a CCD. Wavelength calibration was performed using a combination of spectra from 4-acetamidophenol and sulfur powder. The first set of spectra were collected for all three specimens without polarization selection, using the 2400 lines/mm grating and taking an average of six 5 min acquisition times. Prior to collection, the specimen was scanned with an x-y piezo scan stage over a 20 μm^2 area, with a spectrum acquired every 2.5 μm to determine the sensitivity of the spectra-to-sample heterogeneity and grain size. To assign Raman modes for $Cu_2CdSnTe_4$, a motorized half-wave plate and polarizer were inserted into the path of the incident and scattered light, respectively. Two sets of spectra were collected with the incident and scattered light either parallel or cross polarized. For both the parallel and cross polarization configurations, the half-wave plate and polarizer were rotated simultaneously relative to the sample, while maintaining the parallel and cross-polarized configuration. Each spectrum was collected for 2 min at 40 different angles (every 9°).

Four crystallographic sites form the kesterite unit cell, with Wyckoff positions 2*a* (0, 0, 0) and 2*c* (0, 0.5, 0.25) for Ag or Cu, 2*b* (0.5, 0.5, 0) for Zn, 2*d* (0.5, 0, 0.25) for Sn, and 8*g* (0.756, 0.756, 0.872)[15] for Se atoms, resulting in the well-known layered crystal structure that can be thought of as alternating metal and chalcogenide layers along the *c* axis. There are fifteen Raman-active modes, 3A + 6B + 6E, of the 21 optical vibrational modes at k = 0, not including degeneracies. Figure 2 shows the room temperature Raman spectra of $Cu_2ZnSnSe_4$ and $Ag_2ZnSnSe_4$. The spectra were fit with Lorentzians including a combination of polynomials to account for the fluorescence background. The unknown structure of the fluorescence background contributed to the uncertainty in the amplitudes and widths of the Lorentzians peaks; however, the center frequencies were unique and, for the case of $Cu_2ZnSnSe_4$, were consistent with those previously reported in the literature. The results of our fits to the Raman data are

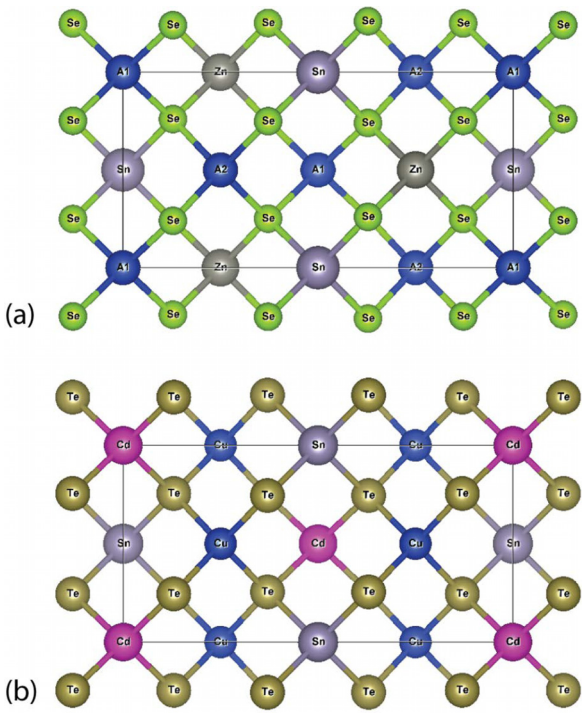

FIG. 1. The (a) kesterite and (b) stannite crystal structures for the compositions discussed in this work, where A represents Cu or Ag in the kesterite structure.

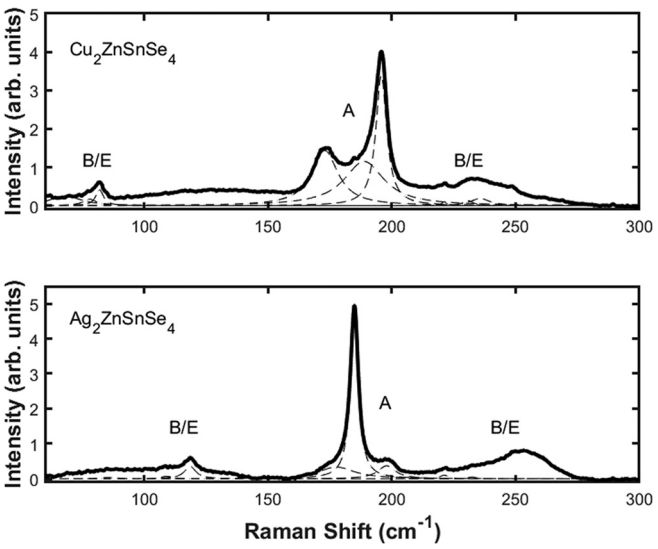

FIG. 2. Raman spectra of (top) $Cu_2ZnSnSe_4$ and (bottom) $Ag_2ZnSnSe_4$ shown with solid lines. The dashed lines indicate the Lorentzian peak fits and are tabulated in Table I.

summarized in Table I. We note that the table compares our data with those of theoretical calculations;[19] however, our mode assignments for $Cu_2ZnSnSe_4$ are in excellent agreement with those obtained from data on single-crystal $Cu_2ZnSnSe_4$.[18]

As shown in Fig. 2 and Table I, the A modes for both $Cu_2ZnSnSe_4$ and $Ag_2ZnSnSe_4$ are not shifted in frequency; however, the low frequency B modes are blue-shifted by over 40 cm^{-1} for $Ag_2ZnSnSe_4$ in comparison to that of $Cu_2ZnSnSe_4$. This frequency shift can be directly related to the metal-metal length difference between $Cu_2ZnSnSe_4$ and $Ag_2ZnSnSe_4$. By replacing Cu with Ag, the size of the unit cell increases from 5.69 Å and 11.34 Å for a (=b) and c, respectively, to 5.99 Å and 11.45 Å, due to the larger size of the Ag atom compared to that of the Cu atom. This relatively large increase in the ab plane, almost 6%, is due to the smaller ionic radius of Cu, which results in a Cu–Se bond length of 2.44 Å, while the larger ionic radius of Ag results in a larger Ag–Se bond length of 2.65 Å.[15] Similarly, the 5.77 Å Cu–Cu distance in $Cu_2ZnSnSe_4$ is much smaller than that for Ag–Ag, 6.09 Å, in $Ag_2ZnSnSe_4$. This significant increase results in a relatively large shift in frequency of the low frequency non-symmetric vibrational modes as they correspond to metal-site vibrations.[19,20] Simultaneous to this change in the ab plane, the expansion along the c axis, i.e., the separation of the Se layers, does not substantially increase from $Cu_2ZnSnSe_4$ to $Ag_2ZnSnSe_4$. Such a small change would therefore not affect the A modes and the higher-frequency B and E modes, as they involve chalcogen vibrations.[19,20] This anisotropic increase in the lattice upon Ag substitution for Cu also encourages stronger interaction between electrons and phonons as well as strongly influences the electronic structure and density of states in these materials.[15]

The composition $Cu_2CdSnTe_4$ forms in the stannite crystal structure with Cu occupying crystallographic position 4d (0, 0.5, 0.25), Cd occupying 2a (0, 0, 0), Sn occupying 2b (0, 0, 0.5), and Te occupying 8i (0.244, 0.244, 0.129)[24] in the unit cell. There are fourteen, $2A_1 + 2B_1 + 4B_2 + 6E$, Raman-active modes for the stannite crystal structure. Experimental Raman spectroscopic data for stannite quaternary chalcogenides have not previously been reported. We therefore employ polarized Raman experiments to assign the symmetry of each mode. In addition, as the mode assignments for kesterite and stannite are similar,[21] due to the similarities in bond lengths and symmetries in these two structure types, we employ a similar analysis as described above in qualitatively comparing our experimental results for $Cu_2CdSnTe_4$ with those for selenium-based theoretical stannite compositions.[19]

Figure 3 shows the Raman spectrum of $Cu_2CdSnTe_4$. From our analyses, we can assign six of the Raman-active modes: 132 cm^{-1} as A_1, 142 cm^{-1} and 149 cm^{-1} as either A_1 or B_1, 68 cm^{-1} and 183 cm^{-1} as B_2, and 196 cm^{-1} as E. These assignments are based on the polarization dependence of each peak as shown in Fig. 4. The peak intensities are plotted as a function of the polarization angle of the incident beam for both parallel and cross polarized configurations. This angular dependence was then fitted to $|e_i \cdot R_{XYZ} \cdot e_s|^2$, where e_i and e_s are the electric field vectors of the incident and scattered beam, respectively, and R_{XYZ} is the appropriate Raman tensor for the stannite structure.[18] The peaks at 68 cm^{-1}, 132 cm^{-1}, and 183 cm^{-1} had a distinctive polarization dependence that could only be fit with B_2, A_1, and B_2, respectively. The peak at 142 cm^{-1} was less clear because fits for the unpolarized spectrum indicated the presence of a shoulder peak at 149 cm^{-1}, as seen in Fig. 3. For this mode, the polarization dependence of each individual contribution could not be determined, presumably due to the polycrystalline nature of the specimen that may have broadened peaks arising from asymmetric modes. Instead, we analyzed the peak intensity of the overall peak. For the parallel configuration, this peak could not be fit to any one mode, but the cross polarized data had a clear B_1 angular dependence. We therefore fit the parallel configuration data to the B_1 mode and found it to fit well but with a large intensity shift, suggesting the additional contribution of an A_1 mode. The fit shown in Fig. 3 is for a superposition of the two modes. This assignment is supported by the fact that two A_1 modes are expected for the stannite structure because the A_1 mode would contribute very little in the cross polarized measurement, which would explain why this mode fits well to the B_1 mode. The phase for the polarization dependence was consistent for all fits within 4.7°, apart from the cross polarized 132 cm^{-1} peak that had very weak intensity. The peak centered at 196 cm^{-1} could be fit as either an A_1 mode or a superposition of E_x and E_y; however, there should only be two A_1 modes for the stannite structure, and the high frequency suggests that an E mode assignment is most likely.

TABLE I. The experimental kesterite $Cu_2ZnSnSe_4$ and $Ag_2ZnSnSe_4$ Raman-active modes, in cm^{-1}, compared to theoretical peak positions for $Cu_2ZnSnSe_4$, from Ref. 19, are tabulated. Similar mode assignments are in the same row for the case of these two quaternary chalcogenides. The first row displays the vibrational mode symmetries for the kesterite crystal structure.

Raman modes	$Cu_2ZnSnSe_4$ theory[a]	$Cu_2ZnSnSe_4$	$Ag_2ZnSnSe_4$
A	178	173	177
	192	189	184
	203	196	198
B (TO LO)	75	68	109
	88	78	118
	187		
	216		
	230		
	237	236	232
E (TO LO)	64		
	81	82	
	174		
	211		
	224	221	221
	239	231	232

[a]Adapted from Ref. 19.

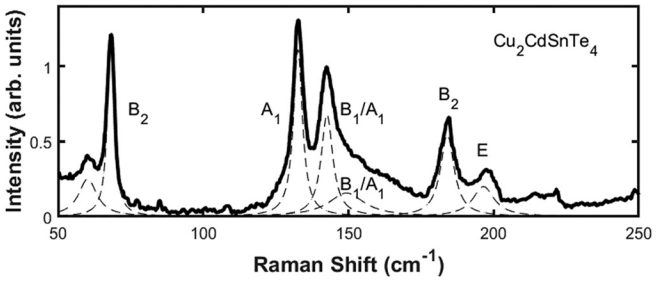

FIG. 3. Raman spectra of $Cu_2CdSnTe_4$ shown with solid lines. The dashed lines indicate the Lorentzian peak fits. These spectra do not include polarization selection.

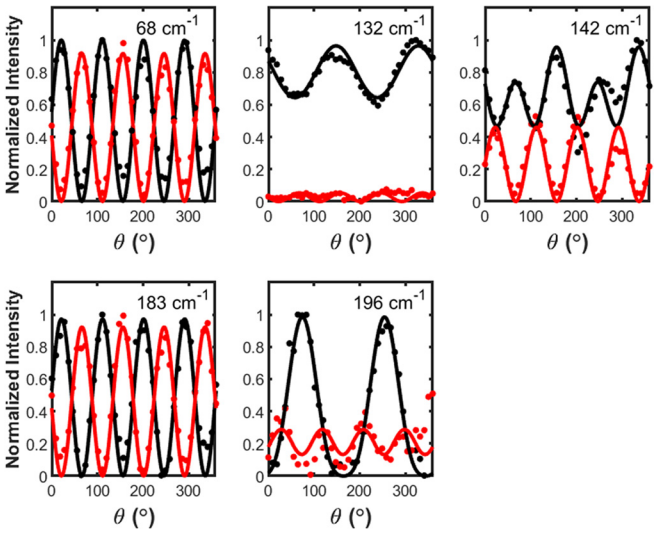

FIG. 4. Polarization dependence of $Cu_2CdSnTe_4$ Raman peak intensities. The parallel and cross polarization intensities are shown with black and red filled circles, respectively. The black and red solid lines are fits that include the Raman tensors of each assigned mode.

As indicated above, and described in the literature, the similarity between the stannite and kesterite structures results in the lack of unequivocal identification by typical powder XRD techniques. The key structural characteristics for both structure types are somewhat similar and can be described by two alternating cation tetrahedral layers along the *c* axis, X and Y or X and Sn for kesterite and X or Y and Sn for stannite (X = Cu or Ag and Y = Zn or Cd). The lattice constants can therefore provide qualitative information of lattice distortion in comparing one material with another. Specifically, we note the symmetric, "breathing," modes in both the kesterite and stannite structures represent vibrational modes of the chalcogen atoms only, in this case selenium (kesterite) and tellurium (stannite). It is therefore instructive to compare these modes between $Cu_2ZnSnSe_4$, or $Ag_2ZnSnSe_4$, and $Cu_2CdSnTe_4$, and note that the symmetric breathing modes shift substantially (over 40 cm^{-1} lower in frequency) for the tellurium-based composition compared to the selenium-based compositions. This is presumably due to the large increase in the lattice parameter upon substitution of Te for Se although both *a* and *c* lattice parameters increase for $Cu_2CdSnTe_4$, $a = 6.198$ Å and $c = 12.25$ Å,[24] as compared to that of the selenium-based compositions (*c* increases by well over 6% compared to $Cu_2ZnSnSe_4$ and by almost 5% compared to $Ag_2ZnSnSe_4$). This increase along the *c* axis significantly affects the symmetric modes in these materials. We further note that our experimentally assigned A_1 modes for $Cu_2CdSnTe_4$ shift by a much larger amount as compared to theoretically calculated frequencies for stannite $Cu_2ZnSnSe_4$, while the non-symmetric modes do not shift nearly as much.[21]

In conclusion, we investigated the Raman-scattering spectra of polycrystalline $Cu_2ZnSnSe_4$, $Ag_2ZnSnSe_4$, and $Cu_2CdSnTe_4$ in order to compare the effect on the optical modes upon metal and chalcogen substitution. For the kesterite compositions, the increase in the bond length upon substitution of Ag for Cu resulted in shifts to much higher frequencies for the non-symmetric modes as they involve metal-site vibrations, whereas the symmetric modes, which involve vibrations of the selenium atoms, do not shift. Conversely, the large anisotropic change in the lattice parameter for the tellurium-based quaternary chalcogenide, in comparison to that of the selenium-based materials, together with the equally significant difference in the mass results in a very large shift of the symmetric modes to lower frequencies. Our results are also corroborated by comparing our mode assignments with those of theoretically calculated optical modes from the literature. These results, together with recent reports on the effect on the electronic structure, bonding, and transport properties of these quaternary chalcogenides upon elemental substitution, reveals the interesting physical properties these materials possess as well as the significant change in properties with stoichiometry. Further computational efforts are needed to provide additional insight into the specific quantitative effects on physical properties from such vibrational frequency shifts.

We acknowledge financial support from the U.S. National Science Foundation under Grant No. DMR-1748188. K.W. acknowledges support from the II-VI Foundation Block-Gift Program.

REFERENCES

[1]C. Rae and F. Bradley, Renewable Sustainable Energy Rev. **16**, 6497 (2012).
[2]M. Bohm, G. Huber, A. MacKinnon, O. Madelung, A. Scharmann, and E.-G. Scharmer, *Physics of Ternary Compounds* (Springer, New York, 1985).
[3]C. H. L. Goodman, J. Phys. Chem. Solids **6**, 305 (1958).
[4]T. Jing, Y. Dai, X. Ma, W. Wei, and B. Huang, J. Chem. Phys. C **119**, 27900 (2015).
[5]P. Qui, X. Shi, and L. Chen, Energy Storage Mater. **3**, 85 (2016).
[6]Y. Dong, L. Wojtas, J. Martin, and G. S. Nolas, J. Mater. Chem. C **3**, 10436 (2015).
[7]W. Wang, M. T. Winkler, O. Gunawan, T. Gokmen, T. K. Todorov, Y. Zhu, and D. B. Mitzi, Adv. Energy Mater. **4**, 1301465 (2014).
[8]X. Li, D. Zhuang, N. Zhang, M. Zhao, X. Yu, P. Liu, Y. Wei, and G. Ren, J. Mater. Chem. A **7**, 9948 (2019).
[9]K. Wei, L. Beauchemin, H. Wang, W. D. Porter, J. Martin, and G. S. Nolas, J. Alloys Compd. **650**, 844 (2015).
[10]Y. Dong, H. Wang, and G. S. Nolas, Phys. Status Solidi RRL **8**, 61 (2014).
[11]M. Ibanez, R. Zamani, A. LaLonde, D. Cadavid, W. Li, A. Shavel, J. Arbiol, J. R. Morante, S. Gorsse, G. J. Snyder, and A. Cabot, J. Am. Chem. Soc. **134**, 4060 (2012).
[12]W. G. Zeier, Y. Pei, G. Pomrehn, T. Day, N. Heinz, C. P. Heinrich, G. J. Snyder, and W. J. Tremel, J. Am. Chem. Soc. **135**, 726 (2013).
[13]Y. Dong, B. Eckert, H. Wang, X. Zeng, T. M. Tritt, and G. S. Nolas, Dalton Trans. **44**, 9014 (2015).
[14]Y. Dong, H. Wang, and G. S. Nolas, Inorg. Chem. **52**, 14364 (2013).
[15]K. Wei, A. R. Khabibullin, T. Stedman, L. M. Woods, and G. S. Nolas, J. Appl. Phys. **122**, 105109 (2017).
[16]K. Wei and G. S. Nolas, ACS Appl. Mater. Interfaces **7**, 9752 (2015).
[17]M. Dimitrievska, F. Boero, A. P. Litvinchuk, S. Delsante, G. Borzone, A. Perez-Rodriguez, and V. Izquierdo-Roca, Inorg. Chem. **56**, 3467 (2017).
[18]D. Nam, J. Kim, J. Lee, A. Nagaoka, K. Yoshino, W. Cha, H. Kim, I. C. Hwang, K. B. Yoon, and H. Cheong, Appl. Phys. Lett. **105**, 173903 (2014).
[19]N. B. M. Amiri and A. Postnikov, Phys. Rev. B **82**, 205204 (2010).
[20]J. M. Skelton, A. J. Jackson, M. Dimitrievska, S. K. Wallace, and A. Walsh, APL Mater. **3**, 041102 (2015).
[21]A. Khare, B. Himmetoglu, M. Johnson, D. J. Norris, M. Cococcioni, and E. S. Aydil, J. Appl. Phys. **111**, 083707 (2012).
[22]K. Wei and G. S. Nolas, J. Solid State Chem. **226**, 215 (2015).
[23]J. Joo, H. B. Na, T. Yu, J. H. Yu, Y. W. Kim, F. Wu, J. Z. Zhang, and T. J. Hyeon, J. Am. Chem. Soc. **125**, 11100 (2003).
[24]Y. Dong, K. Wei, Z. H. Ge, A. R. Khabibullin, J. Martin, J. R. Salvador, L. M. Woods, and G. S. Nolas, Appl. Phys. Lett. **104**, 252107 (2014).
[25]T. Maeda, S. Nakamura, and T. Wada, Thin Solid Films **519**, 7513 (2011).